Log-Domain Wavelet Bases

Sandro A. P. Haddad, *Student Member, IEEE*, Sumit Bagga, *Student Member, IEEE*, and Wouter A. Serdijn, *Member, IEEE*

***Abstract*—A novel procedure to approximate wavelet bases using analog circuitry is presented. First, an approximation is used to calculate the transfer function of the filter, whose impulse response is the required wavelet. Next, for low-power low-voltage applications, we optimize the state-space description of the filter for dynamic range, sensitivity and sparsity requirements. The filter design that follows is based on an orthonormal ladder structure with log-domain integrators as the main building blocks. Simulations demonstrate that it approximates the required wavelet base (i.e., Morlet) in an excellent way. The circuit operates from a 1.2-V supply voltage and a bias current of 1.2 μA.**

***Index Terms*—Analog electronics, log-domain filters, orthonormal ladder filter, wavelet transform (WT).**

I. Introduction

FOR signal processing, the wavelet transform (WT) has been shown to be a very promising mathematical tool [1]–[3], particularly for local analysis of nonstationary and fast transient signals, due to its good estimation of time and frequency localizations. Wavelet analysis is performed using a prototype function called the wavelet base, which decomposes a signal into components appearing at different scales (or resolutions). Often, systems employing the WT are implemented using digital signal processing. However, in ultra low-power applications such as biomedical implantable devices [4]–[6], it is not suitable to implement the WT by means of digital circuitry due to the high power consumption associated with the required analog–digital (A/D) converter. In [7], we proposed a method for implementing the WT in an analog way. However, besides the derivatives of the Gaussian wavelet presented in [7], there are several families of wavelets that have proven to be especially useful [1]. Therefore, this paper presents a more general procedure to obtain various types of wavelet bases.

Section II treats the basic theory of the WT. Section III deals with the computation of a transfer function which describes a certain wavelet base that can be implemented as an analog filter. Section IV describes the complete filter design, taking into account the requirements for low-power low-voltage applications. Subsequently, the dynamic range (DR) is optimized and log-domain integrators are implemented to face the ultra low-power challenges Some results provided by simulations are given in Section V. Finally, Section VI presents the conclusions.

Manuscript received March 2, 2004; revised August 20, 2004 and February 11, 2005. This work is part of the BioSens project supported by STW, the Dutch Technology Foundation. This paper was recommended by Associate Editor I. M. Filanovsky.

The authors are with the Electronics Research Laboratory, Faculty of Electrical Engineering, Mathematics and Computer Science, Delft University of Technology, Delft 2628 CD, The Netherlands (e-mail: s.haddad@ewi.tudelft.nl).

Digital Object Identifier 10.1109/TCSI.2005.853360

II. Wavelet Transform

The WT is a linear operation that decomposes a signal into components that appear at different scales (or resolutions) [2]. The WT is a so-called constant-Q analysis. The WT of a function at the scale a and position τ is given by

$$C(\tau, a) = \frac{1}{\sqrt{a}} \int_{-\infty}^{\infty} x(t)\psi^* \left(\frac{t-\tau}{a} \right) dt \tag{1}$$

where $\psi(t)$ is the wavelet base (or mother wavelet) and $*$ denotes the complex conjugation. The factor $1/\sqrt{a}$ is used for energy normalization. Hence, the WT is based on the convolution of the signal with a dilated impulse response of a filter (defined by $\psi(t)$), mapping the signal onto a two-dimensional function of time and frequency. The main idea of the WT is to look at a signal at various windows and analyze it with various resolutions. It provides an alternative to the classical short-time Fourier transform (STFT) or Gabor transform [3]. In contrast to the STFT, which uses a single analysis window, the WT uses short windows (small a) at high-frequency analysis and long windows (large a) at low-frequency analysis. The time-frequency plane of a WT is shown in Fig. 1(a). As one can see, the time-frequency (or time-scale) representation has an intrinsic limitation: the product of the resolution in time and frequency is limited by the uncertainty principle (Heisenberg inequality) [3]. It means that one can only trade time resolution for frequency resolution and vice versa. Furthermore, in order to avoid redundancy, one can sample the scale parameter along the dyadic sequence $(2^j)_{j\in Z}$, i.e., $a = 2^j$ [2].

The wavelet analysis is performed using a prototype function called the wavelet base, $\psi(t)$ ($\psi(t) \in L^2$). The main characteristic of the wavelet base is given by

$$\int_{-\infty}^{\infty} \psi(t)dt = 0. \tag{2}$$

This means that the wavelet base is oscillatory and has zero mean value. Also, this function needs to satisfy the admissibility condition so that the original signal can be reconstructed by the inverse WT

$$\int_{-\infty}^{\infty} \frac{|\Psi(\omega)|^2}{|\omega|} d\omega = C_\Psi < \infty \tag{3}$$

where $\Psi(\omega)$ is the Fourier transform of the wavelet base $\psi(t)$. The admissible condition implies that the Fourier transform of the wavelet must have a zero component at zero frequency. Hence, the wavelets are inherently bandpass filters in the Fourier domain, defined as wavelet filters. Any function that has finite energy is square integrable and satisfies the wavelet

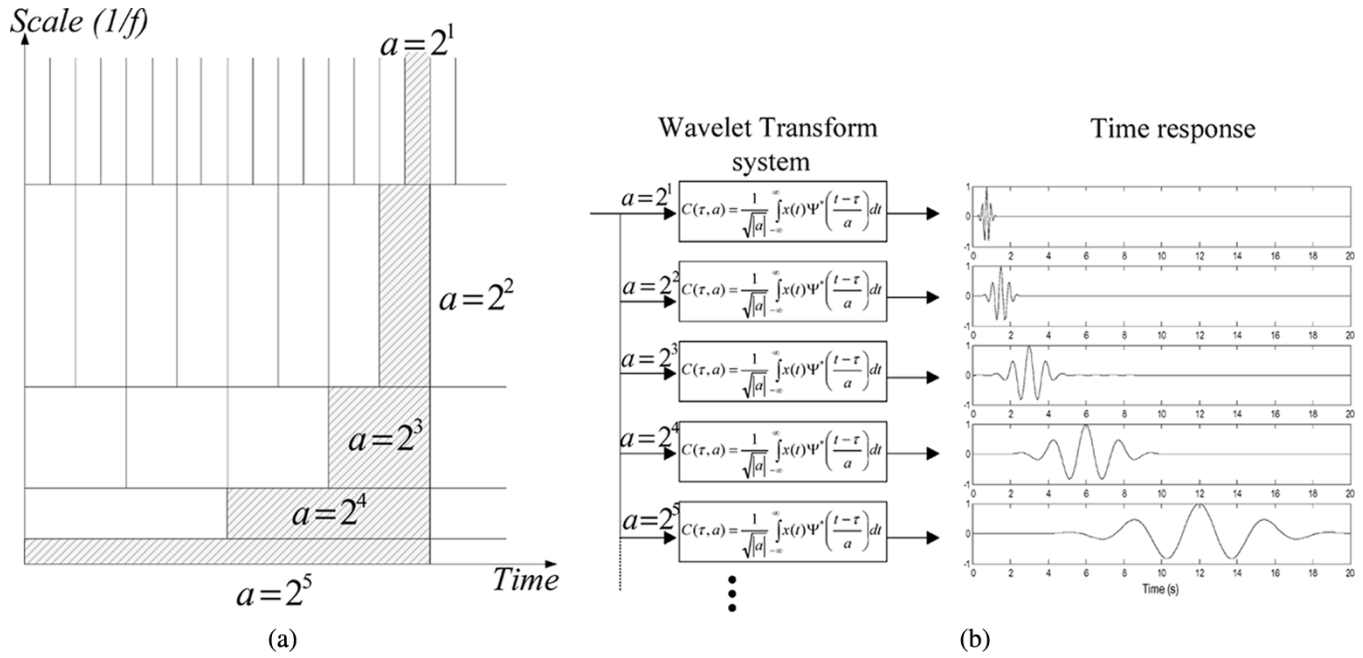

Fig. 1. WT system. (a) Time-frequency plane. (b) Morlet WT system with multiple scales.

admissibility condition can be a wavelet [1]. Fig. 1(b) shows a wavelet system with multiple scales in parallel that can be used to compute the WT in real time. As an example, a Morlet WT system has been presented.

III. Wavelet Bases Approximation

Log-domain filters and analog filters in general are described mathematically by either linear differential equations of finite order in the time domain, or rational transfer functions in the Laplace domain. Hence, in order to implement the wavelet filter one must first derive these respective differential equations. However, a linear differential equation having a predefined desired impulse response does not always exist. Hence, one is obliged to use a suitable approximation method. In addition, any approximation method should be associated with some measure of error. Therefore, we define an error criterion based on the mean-square error (MSE) [8] which is defined as

$$\mathrm{MSE} = \frac{1}{b-a}\int_a^b |h(t) - h'(t)|^2\, dt \tag{4}$$

where $h(t)$ and $h'(t)$ are the desired impulse response and the approximated impulse response, respectively. Nonetheless, one of the most important aspects of an analog filter synthesis is that the approximating function must lead to a physically realizable network which is dynamically stable. There are several mathematical techniques that are frequently used to achieve the best approximation possible [9]. A method which has proven to be successful is the Padé approximation in the Laplace domain of the impulse response of the filter [9].

A. Padé Approximation in Laplace Domain

Just like the Taylor expression, the Padé approximation is an approximation that concentrates around one point of the function that needs to be approximated [10]. In the Padé approximation, the coefficients of the approximating rational expression are computed from the Taylor coefficients of the original function. If we were to apply the Padé approximation to $h(t)$ in the time domain, we would have to transform this function to the Laplace domain, which would possibly yield difficult expressions or even a noncausal or unstable filter.

The reason to apply the Padé approximation to the Laplace transform of $h(t)$ is that it immediately yields a rational expression which is suitable for implementation. Hence, a Padé approximation of $H(s)$ represents the transfer function of a possible filter. If the approximation rational function has a numerator of order m and a denominator of order n, the original function can be approximated up to order $m+n+1$.

Now, we will derive the Padé approximation of a general function $f(t)$. Suppose that we have the Taylor series expansion of $F(s)$ around some point, e.g., $s=0$, then

$$F(s) = c_0 + c_1 s + \cdots + c_k s^k + O(s^{k+1}). \tag{5}$$

The constants c_0 to c_k are called the Taylor coefficients of $F(s)$. Unfortunately, $F(s)$ is not a suitable expression to build a filter, since it has only zeros. Therefore, to solve this problem, we apply a Padé approximation of function $F(s)$ which is given by

$$\hat{F}(s) = \frac{P(s)}{Q(s)} = \frac{p_0 + p_1 s + \cdots + p_m s^m}{q_0 + q_1 s + \cdots + q_n s^n} \tag{6}$$

where $\hat{F}(s)$ is the truncated Taylor series given by (5) with $k = m+n$. The coefficients of $P(s)$ can be computed as follows. When a product of two polynomials is taken, the coefficients of the product polynomial can be computed by taking the convolution of the coefficients of both factors. Thus, the coefficients of $P(s)$ can be computed from the convolution of the

Taylor coefficients of $\hat{F}(s)$ with the finite number of coefficients of $Q(s)$. We can write this convolution in a matrix-vector form

$$[\hat{F}]\cdot[Q]=[P]\rightarrow\begin{bmatrix}c_0 & 0 & \dots & 0\\ c_1 & c_0 & & \vdots\\ \vdots & c_1 & \ddots & 0\\ \vdots & \vdots & \ddots & c_0\\ \vdots & \vdots & & c_1\\ \vdots & \vdots & & \vdots\\ c_k & c_{k-1} & \dots & c_{k-n}\end{bmatrix}\cdot\begin{bmatrix}q_0\\ q_1\\ \vdots\\ q_n\end{bmatrix}=\begin{bmatrix}p_0\\ p_1\\ \vdots\\ \vdots\\ \vdots\\ p_k\end{bmatrix}. \tag{7}$$

As the entries of $[\hat{F}]$ are given by the Taylor coefficients of $F(s)$, the entries of $[P]$ depend only on the choice of $[Q]$. In other words, the choice of $[Q]$ is determined by the restrictions on $[P]$. Note that the desirable value of $[P]$ is defined by two constraints: i) k should be as large as possible, since this gives the most accurate approximation; ii) $P(s)$ should have the desired order m $(m\leq n)$ for a causal filter.

From these constraints it can be concluded that the coefficients p_{m+1} to p_k should be zero. Let $[\hat{F}]_{m+1,k}$ denote the submatrix of $[\hat{F}]$, containing rows $m+1$ to k of $[\hat{F}]$. Then $[Q]$ can be expressed as

$$\begin{bmatrix}p_{m+1}\\ \vdots\\ p_k\end{bmatrix}=[\hat{F}]_{m+1,k}\cdot[Q]=0 \tag{8}$$

which yields

$$\underline{q}\in\text{Nullspace}\begin{bmatrix}c_{m+1} & \dots & c_0 & 0\\ c_{m+2} & & c_1 & c_0\\ \vdots & & & \vdots\\ c_{m+n} & \dots & & c_m\end{bmatrix} \tag{9}$$

with $q_n=1$ for normalization. Finally, the coefficients of $[P]$ are defined by

$$\begin{bmatrix}p_0\\ p_1\\ \vdots\\ p_m\end{bmatrix}=\begin{bmatrix}c_0 & 0 & \dots & 0\\ c_1 & c_0 & & \vdots\\ \vdots & c_1 & \ddots & 0\\ \vdots & \vdots & \ddots & c_0\\ \vdots & \vdots & & c_1\\ \vdots & \vdots & & \vdots\\ c_m & c_{m-1} & \dots & c_{m-n}\end{bmatrix}\cdot\begin{bmatrix}q_0\\ q_1\\ \vdots\\ q_n\end{bmatrix} \tag{10}$$

with $c_k=0$ for $k<0$. Then, if the approximating rational function has a numerator of order m and a denominator of order n, the original function can be approximated up to order $m+n+1$. For instance, one can apply the Padé function to approximate the first or the second derivative of a Gaussian as seen in Fig. 2. We apply a [6/10] Padé approximation, i.e., $m=6$ and $n=10$, which yields an approximation of order $k=16$ of the Taylor series expansion, resulting in an MSE of $0.19\cdot10^{-4}$ and $0.548\cdot10^{-3}$ for the first and the second derivative, respectively. In Table I one can see the Taylor and Padé coefficients of both functions.

However, the Padé approximation has some convergence problems when one tries to approximate a function with many oscillations, such as the Morlet wavelet. Therefore, the next section will describe an implementation of the procedure to obtain a stable transfer function for these kinds of wavelet bases. In this way, it presents a generalized procedure for implementing analog filters of various types of wavelet bases.

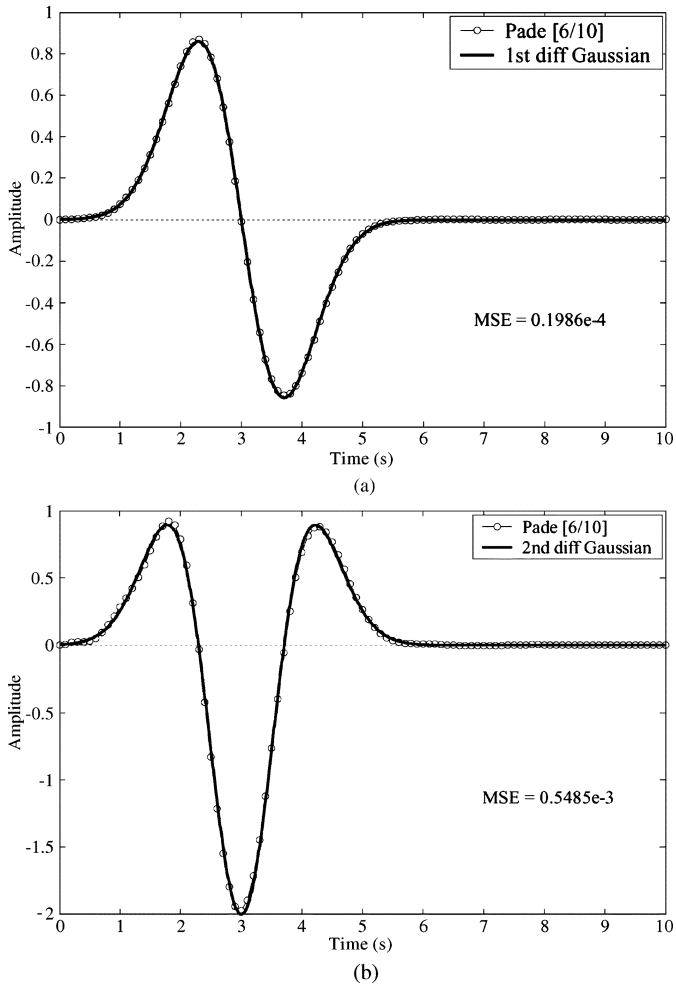

Fig. 2. Impulse response approximation using Padé [6/10]. (a) First derivative of Gaussian. (b) Second derivative of Gaussian.

B. Wavelet Filter Approach

The proposed procedure that generates a transfer function of a wavelet base can be seen in the flowchart in Fig. 3. The procedure is based on the Padé approximation described in the previous section. The starting point is the definition of an expression in the time domain which represents the wavelet under investigation. If the wavelet base does not have an explicit expression (e.g., Daubechies wavelets), then the splines interpolation method [8] is used. Subsequently, one determines the appropriate envelope to set the width of the wavelet. Once again, if the envelope does not have an explicit expression, the splines interpolation is applied. In this paper, the Gaussian pulse was chosen as the envelope, which is perfectly local in both the time and frequency domain. Once the envelope has been defined, the Padé approximation is executed to find a stable and rational transfer function that is suitable for implementation as an analog filter. As the main advantage of the Padé method is its

TABLE I
TAYLOR AND PADÉ COEFFICIENTS OF THE FIRST AND THE SECOND DERIVATIVE OF GAUSSIAN

	1st diff. Gaussian		2nd diff. Gaussian	
Expression (time)	$\psi(t) = -2(t-3)e^{-(t-3)^2}$		$\psi(t) = (-2+4(t-3)^2)e^{-(t-3)^2}$	
Taylor expansion (Laplace domain) $k = 16$	$\hat{F}(s) = -0.0001 + 1.77s - 5.31s^2 + 8.41s^3 - 9.3s^4 + 8.03s^5 - 5.74s^6 + 3.54s^7 - 1.92s^8 + 0.94s^9 - 0.42s^{10} + 0.17s^{11} - 0.066s^{12} + 0.023s^{13} - 0.008s^{14} + 0.002s^{15} - 0.007s^{16}$		$\hat{F}(s) = -0.0007 - 0.0001s + 1.77s^2 - 5.31s^3 + 8.41s^4 - 9.3s^5 + 8.03s^6 - 5.74s^7 + 3.54s^8 - 1.92s^9 + 0.94s^{10} - 0.42s^{11} + 0.17s^{12} - 0.066s^{13} + 0.023s^{14} - 0.008s^{15} + 0.002s^{16}$	
[Q] coefficients $n = 10$	$q_0 = 38.6 \cdot 10^3$ $q_1 = 103.6 \cdot 10^3$ $q_2 = 130.5 \cdot 10^3$ $q_3 = 102.2 \cdot 10^3$ $q_4 = 55.3 \cdot 10^3$ $q_5 = 21.7 \cdot 10^3$	$q_6 = 6.3 \cdot 10^3$ $q_7 = 1.35 \cdot 10^3$ $q_8 = 205.6$ $q_9 = 20.27$ $q_{10} = 1$	$q_0 = 37.8 \cdot 10^3$ $q_1 = 100.7 \cdot 10^3$ $q_2 = 126.4 \cdot 10^3$ $q_3 = 98.6 \cdot 10^3$ $q_4 = 53.3 \cdot 10^3$ $q_5 = 20.9 \cdot 10^3$	$q_6 = 6.1 \cdot 10^3$ $q_7 = 1.30 \cdot 10^3$ $q_8 = 199.7$ $q_9 = 19.91$ $q_{10} = 1$
[P] coefficients $n = 6$	$p_0 = -4.77$ $p_1 = 68.5 \cdot 10^3$ $p_2 = -22 \cdot 10^3$ $p_3 = 6.1 \cdot 10^3$	$p_4 = -576.95$ $p_5 = 44.67$ $p_6 = 5.81$	$p_0 = -4.67$ $p_1 = -13.21$ $p_2 = 11.1 \cdot 10^3$ $p_3 = -3.7 \cdot 10^3$	$p_4 = 1.08 \cdot 10^3$ $p_5 = -131.28$ $p_6 = 13.54$

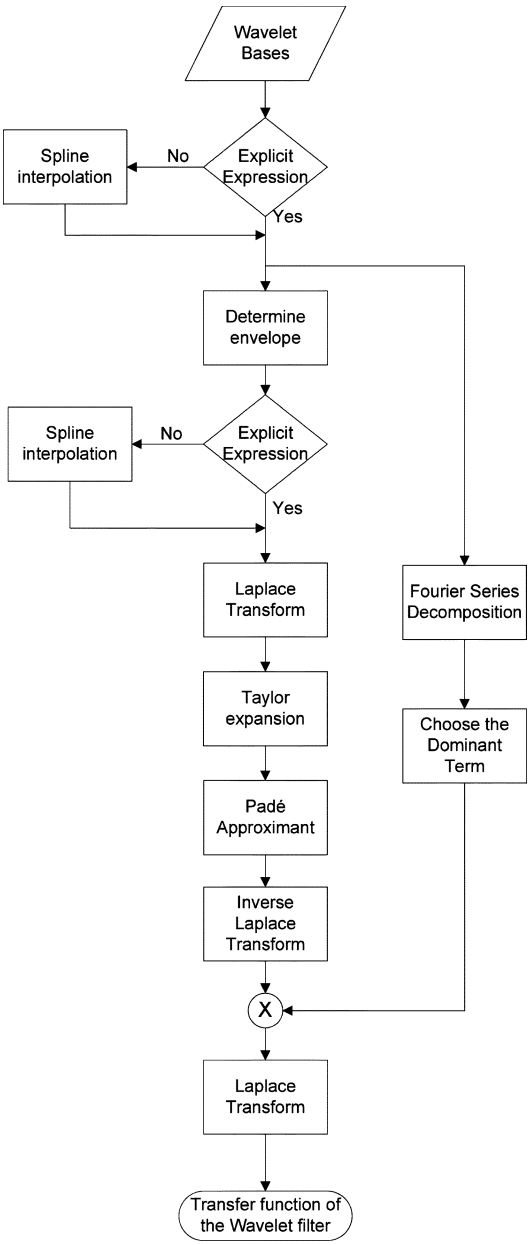

Fig. 3. Flowchart of the wavelet filter approach.

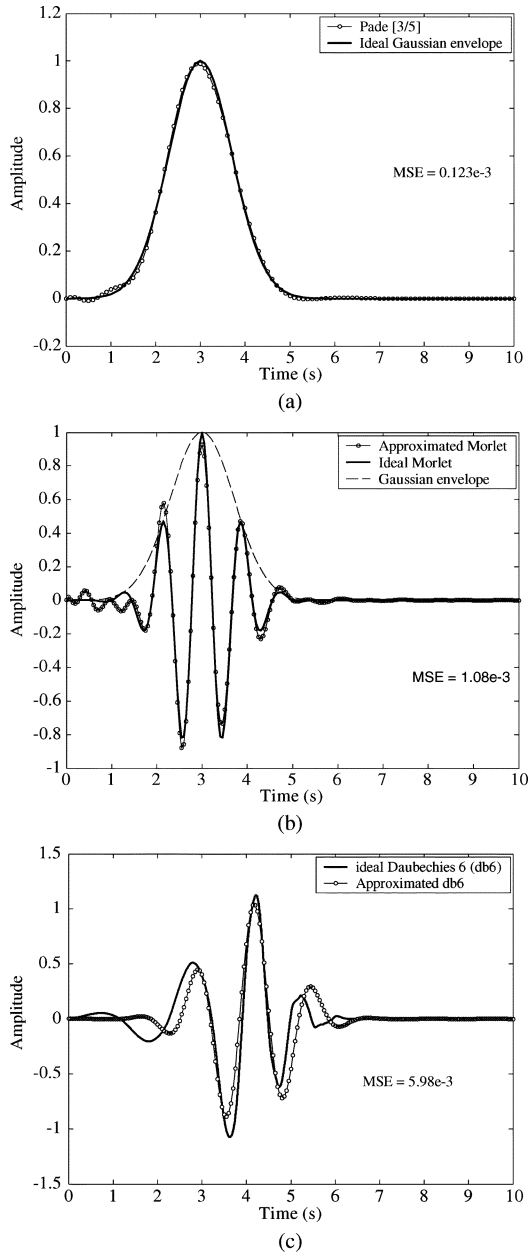

Fig. 4. Impulse response of the wavelet filters, the ideal impulse (dashed line) and the approximated impulse (solid line). (a) Gaussian envelope, (b) Morlet. (c) db6 wavelet base.

TABLE II
MORLET WAVELET BASE APPROACH PARAMETERS

	Morlet wavelet base
Expression (time)	$\psi(t) = cos(5\sqrt{2}t)e^{-(t-3)^2}$
Envelope	Gaussian $\Rightarrow e^{-(t-3)^2}$
Fourier Series (Dominant term)	$cos(5\sqrt{2}t)$
Padé [3/5](Gaussian)	$H_{gaussian}(s) = \frac{-1.31s^3+8.82s^2-25.11s+31.74}{s^5+6.66s^4+21.14s^3+38.59s^2+39.56s+17.91}$
Morlet transfer function	$H(s) = \mathcal{L}\{\mathcal{L}^{-1}\{H_{gaussian}(s)\} \times cos(5\sqrt{2}t)\}$ $H(s) = \frac{0.9s^8-13s^7+177s^6-618s^5+345s^4+7\cdot10^4s^3-4\cdot10^5s^2+2\cdot10^6s-3\cdot10^6}{s^{10}+13s^9+336s^8+3\cdot10^3s^7+4\cdot10^4s^6+2\cdot10^5s^5+2\cdot10^6s^4+8\cdot10^6s^3+4\cdot10^7s^2+9\cdot10^7s+3\cdot10^8}$

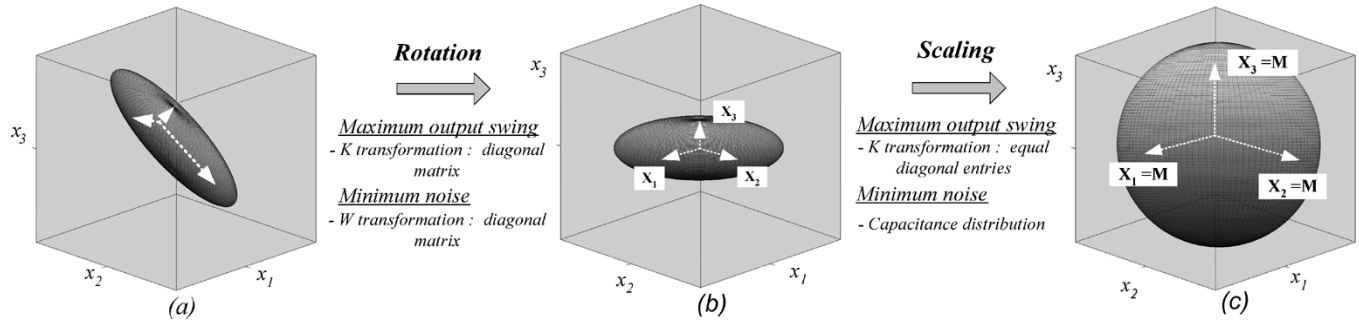

Fig. 5. DR optimization based on the similarity transformation of K and W and capacitance distribution. The coordinate axes represent the state variables and the cuboid represents the maximum signal amplitude (M) that the integrators are able to handle. (a) The initial state space representation (ellipsoid) is usually not well adapted to the integrator's representations capacity bounds (cuboid). (b) The (rotated) ellipsoid's principal axes are now aligned to the coordinate axes, as a result of the diagonalization procedure to the matrices K and W. (c) Finally, the optimized state representation is obtained by scaling the states variables. Note that the sphere represents the maximum possible mean square radius which can be fitted into the integrator's capacity cuboid.

computational simplicity and its general applicability [10], it can easily be applied to other envelopes as well. The Padé approximation is preceded by a two-step procedure. First, a Laplace transform is executed, and then a Taylor expansion is performed on the expression of the envelope in the Laplace domain. Finally, the wavelet is decomposed into a Fourier series to find the dominant term (the term with the largest coefficient) such that when multiplied with the envelope in the time domain, it results in the approximated wavelet base. The results obtained from the use of this method are illustrated in Fig. 4, where the Morlet and the Daubechies (db6) wavelet bases have been approximated, respectively. Other wavelet bases can also be approximated in a similar manner. The rest of this paper will describe the design of a Morlet wavelet filter. The related expression of the Morlet wavelet base approach, the Padé expression of the envelope function and, the transfer function of the Morlet wavelet filter are given in Table II. $\mathcal{L}$ and $\mathcal{L}^{-1}$ represent the Laplace transform and the inverse Laplace transform, respectively.

In the next section, we will map the transfer function onto a state space description that is suitable for low-power implementation.

IV. FILTER DESIGN

There are many possible state space descriptions for a circuit that implements a certain transfer function. The same holds for practical realizations. This allows the designer to find a circuit that fits his specific requirements. In the context of low-power, low-voltage analogue integrated circuits, the most important requirements are the DR, the sensitivity, and the sparsity, all of which will be treated in the subsections that follow. We will focus on a synthesis technique that is exclusively based on integrators.

A. DR

A system's DR is essentially determined by the maximum processable signal magnitude and the internally generated noise. It is well known that the system's controllability and observability gramians play a key role in the determination and optimization of the DR [11], [12]. The controllability (K) and observability (W) gramians are derived from the state space description and are computed by solving the equivalent Lyapunov equations

$$AK + KA^T + 2\pi BB^T = 0 \tag{11}$$

$$A^TW + WA + 2\pi C^TC = 0 \tag{12}$$

where A, B, and C are the state, input, and output matrices of the state-space description, respectively. The entries of A, B, and C are derived directly from the coefficients of the transfer function.

As the DR of a circuit is defined as the ratio of the maximum and the minimum signal level that it can process, optimization of the DR is equivalent to the simultaneous maximization of the (distortionless) output swing and the minimization of the overall noise contribution. In [13], Rocha gives a geometric interpretation of the optimization of the DR. A visualization of the optimization procedure can be seen in Fig. 5, for a system with three state variables. The output swing is related via the controllability gramian to the space of "occurring" state-space vectors. Under the assumption of a random input signal, the shape of this space is generally a multidimensional ellipsoid. The constraint that each integrator has a maximum representation capacity (M) defines a multidimensional cuboid, which, for a distortionless transfer, should contain the former mentioned ellipsoid completely. As the mean square radius of the ellipsoid is equivalent to the maximum output swing, the output swing is maximal

when the mean square radius is. This can occur if and only if the ellipsoid becomes a spheroid. In that case, the controllability gramian is a diagonal matrix with equal diagonal entries, which means that all axes of the ellipsoid have equal length. Thus, the first optimization step boils down to a similarity transform, such that the controllability gramian of the new system becomes a diagonal matrix with equal diagonal entries. In the second step of the optimization procedure, the system is optimized with respect to its noise contribution. Rocha defines another ellipsoid, which describes the noise that is added to the state vector in each direction. While preserving the result of the first optimization step, it is possible to rotate the state space, such that the observability gramian becomes a diagonal matrix as well. In that case, the axes of the noise ellipsoid are aligned with the "system axes."

In [13] it is shown that, in order to maximize the DR of the system, one should minimize the objective functional, which represents the relative improvement of the DR and contains all parameters which are subject to manipulation by the designer. The objective functional is given by

$$F_{\mathrm{DR}} = \frac{\max_i k_{ii}}{(2\pi)^2} \sum_i \frac{\alpha_i}{C_i} w_{ii} \tag{13}$$

where k_{ii} and w_{ii} are the main diagonal elements of K and W, respectively, $\alpha_i = \sum_j |A_{ij}|$ is the absolute sum of the elements on the i-th row of A, and C_i is the capacitance in integrator i.

Finally, profiting from the well-known fact that the relative noise contribution of an integrator decreases when the capacitance and bias current increase, we match the optimal capacitance distribution to the noise contributions of each individual integrator (noise scaling), i.e, the diagonal entries of W, combined with the coefficients in matrix A, which is defined by [13], resulting in

$$C_i = \frac{\sqrt{\alpha_i w_{ii} k_{ii}}}{\sum_j \sqrt{\alpha_j w_{jj} k_{jj}}}. \tag{14}$$

Applying the optimization method described in [13] for the transfer function given in Section III, we find that F_{DR} equals 96.98, which is the absolute minimum value of the objective functional associated with this transfer function.

B. Sparsity

The drawback of a DR optimal system is that its state-space matrices are generally fully dense, i.e., all the entries of the A, B, C matrices are filled with nonzero elements. These coefficients will have to be mapped onto circuit components, and will result in a complex circuit with a large number of interconnections. For high-order filters it is therefore necessary to investigate how a realization of the desired transfer function having sparser state-space matrices would compare to the one having maximal DR. For a less complex circuit, it is possible, for instance, to reduce A to upper triangular by a Schur decomposition and by this reducing the number of nonzero coefficients in A [13]. However, this transformation leads to an increase in the system noise and consequently to an increase in the objective functional in (13). Another possibility is the Orthonormal Ladder structure [14], which is significantly sparser than the fully dense A matrix of the DR optimal system and the Schur decomposition. The advantage of using this structure is its low sensitivity to coefficient mismatch; it will be described in the next section.

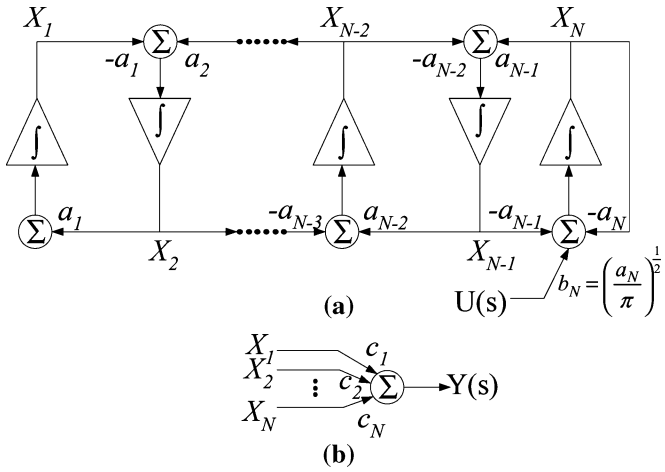

Fig. 6. Block diagram of an orthonormal ladder filter. (a) Leapfrog structure. (b) Output summing stage.

C. Orthonormal Ladder Structure

When designing high-order filters, it is very desirable to concentrate on circuits that are less sensitive to component variations. It is known that an optimal DR system will also have optimal sensitivity [15]. Nevertheless, in order to improve the state-space matrices' sparsity, an orthonormal ladder structure will be implemented, which still presents a good behavior with respect to sensitivity. Fig. 6 shows a block diagram of a general orthonormal ladder filter [14]. As shown in the block diagram, the filter output is obtained from a linear combination of the outputs of all integrators.

The A, B, and C matrices of this structure for the defined transfer function are given by (15), shown at bottom of the next page.

The A matrix is tridiagonal and is very nearly skew-symmetric except for a single nonzero diagonal element. The B vector consists of all zeros except for the Nth element. Another property of orthonormal ladder filters is the fact that the resulting circuits are inherently state scaled, i.e., the controllability gramian is already an identity matrix. The drawback of this structure is that the system is not optimized with respect to its noise contribution. However, if an optimal capacitance distribution is applied to this suboptimal system, it can still yield some extra gain compared to the case of equal capacitances. In this case, the objective functional becomes $F_{\mathrm{DR}} = 147.90$, which is not so far from the optimum case. The DR has decreased by only 1.83 dB. Finally, the normalized capacitance distribution is given by

$$(C_1, \ldots, C_{10}) = C'(0.142,\ 0.162,\ 0.110,\ 0.117,\ 0.086,\ 0.091,\ 0.073,\ 0.080,\ 0.073,\ 0.061)$$

where C' represents the unit-less value of the total capacitance when expressed in F. The next section will present the log-domain integrator, which is the basic building block of the filter.

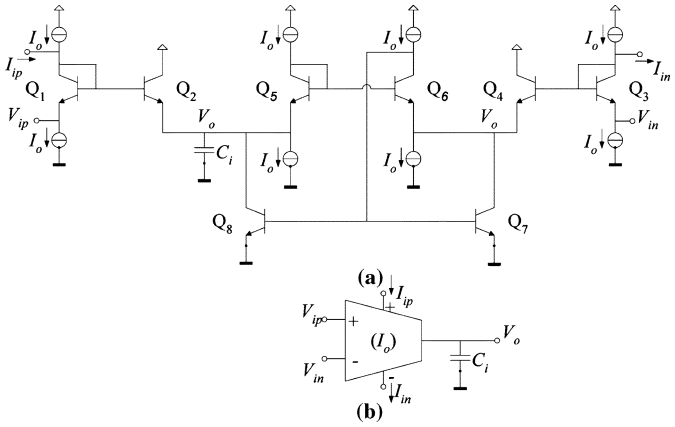

Fig. 7. (a) The multiple-input low power log-domain integrator and (b) its symbol [16].

D. Low-Power Log-Domain Integrator

The trend toward lower power consumption, lower supply voltage and higher frequency operation has increased the interest in new design techniques for analogue integrated filters. The class of translinear (TL) filters, also known as log-domain filters, has emerged in recent years as a promising approach to face these challenges. The TL approach is inherently companding and exploits the exponential large-signal transfer function of the semiconductor devices to implement a desired linear or nonlinear differential equation.

A simple bipolar multiple-input low-power log-domain integrator [16] will be used as the basic building block for the implementation of the state space equation of the wavelet filter described in the previous section. This log-domain integrator is shown in Fig. 7 [16]. A pair of log-domain cells with opposite polarities and an integrating capacitor form the core of the integrator. V_{ip} and $V_{\rm in}$ are the noninverting and inverting input voltages, respectively, and the input currents are I_{ip} and $I_{\rm in}$, which are superimposed on the dc bias currents. The output voltage V_o is given by the voltage across the capacitor. The circuit is composed of two identical log-domains cells, a voltage buffer, and a current mirror. The log-domain cells Q_1-Q_2 and Q_3-Q_4 generate the log-domain currents I_{c2} and I_{c4}, respectively. A voltage buffer realized by Q_5-Q_6 is inserted between them. Therefore, the output log-domain voltage V_o at the emitter of Q_2 also appears at the emitter of Q_4. Finally, to obtain a log-domain integrator equation, we used a current mirror Q_7-Q_8 to realize the difference between the two log-domain currents on the capacitor node. The connection from the bases of transistors Q_7 and Q_8 to the collector of Q_6 closes the feedback loop around Q_6 and Q_7. This connection is convenient because it ensures that the overall voltage headroom is minimized. The equation that relates the input and output voltages to the current flowing in the integrating capacitor becomes

$$C_i \frac{dV_o}{dt} = (I_o + I_{ip}) e^{\frac{V_{ip}-V_o}{V_T}} - (I_o + I_{\rm in}) e^{\frac{V_{\rm in}-V_o}{V_T}}. \qquad (16)$$

Notice that the input and output voltages of the integrator are at the same dc level. Therefore, log-domain filter synthesis can easily be achieved by direct coupling of these integrators.

E. Synthesis of the Log-Domain State-Space Filter

By applying a simple mapping to the linear state-space (15), we can obtain the corresponding log-domain circuit realization which employs the log-domain integrator cell introduced in the previous section [17].

The block diagram of the log-domain implementation of (15) is illustrated in Fig. 8, using the universal log-domain cell symbol described in [17] and shown in Fig. 7(b). Note that each column of the filter structure corresponds to a row in the state-space formulation. The parameter A_{ij} is implemented by

$$A = \begin{bmatrix} 0 & 6.5 & 0 & 0 & 0 & 0 & 0 & 0 & 0 & 0 \\ -6.5 & 0 & 1.8 & 0 & 0 & 0 & 0 & 0 & 0 & 0 \\ 0 & -1.8 & 0 & 6.6 & 0 & 0 & 0 & 0 & 0 & 0 \\ 0 & 0 & -6.6 & 0 & 2.7 & 0 & 0 & 0 & 0 & 0 \\ 0 & 0 & 0 & -2.7 & 0 & 6.4 & 0 & 0 & 0 & 0 \\ 0 & 0 & 0 & 0 & -6.4 & 0 & 3.9 & 0 & 0 & 0 \\ 0 & 0 & 0 & 0 & 0 & -3.9 & 0 & 6.3 & 0 & 0 \\ 0 & 0 & 0 & 0 & 0 & 0 & -6.3 & 0 & 5.9 & 0 \\ 0 & 0 & 0 & 0 & 0 & 0 & 0 & -5.9 & 0 & 10.5 \\ 0 & 0 & 0 & 0 & 0 & 0 & 0 & 0 & -10.5 & -13.3 \end{bmatrix}$$

$$B = \begin{bmatrix} 0 \\ 0 \\ 0 \\ 0 \\ 0 \\ 0 \\ 0 \\ 0 \\ 0 \\ 2.05 \end{bmatrix}$$

$$C = [0.75 \ -1.34 \ 0.75 \ 0.68 \ -0.57 \ 0.44 \ -0.002 \ -0.10 \ 0.04 \ 0] \qquad (15)$$

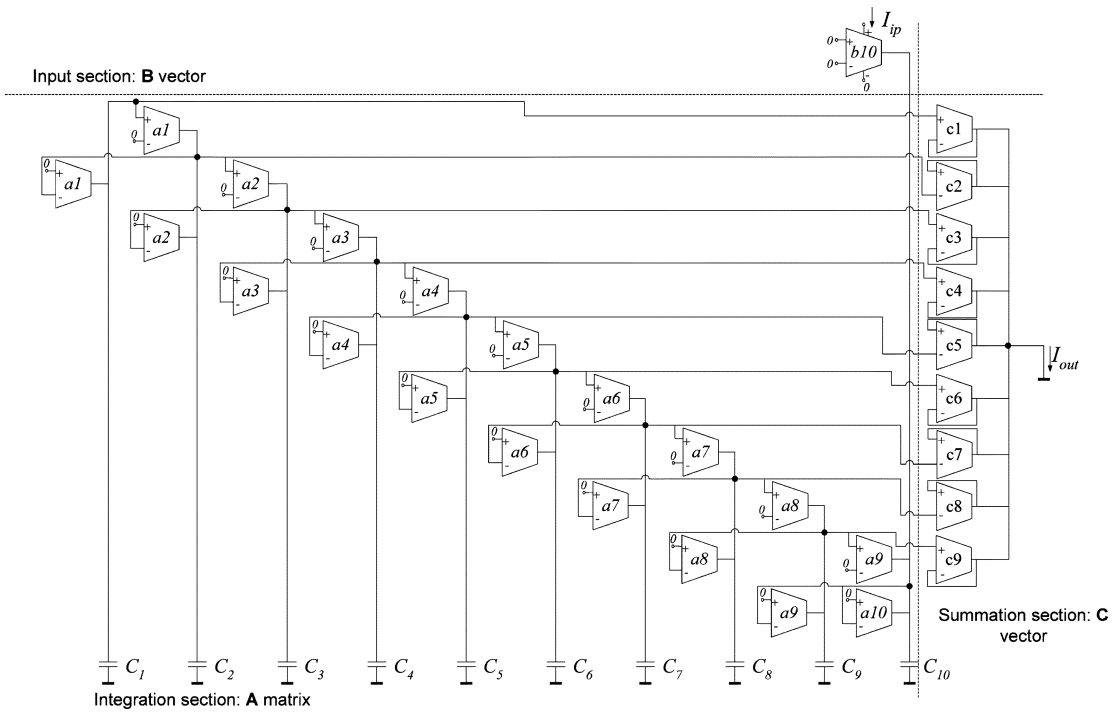

Fig. 8. Complete state-space filter structure.

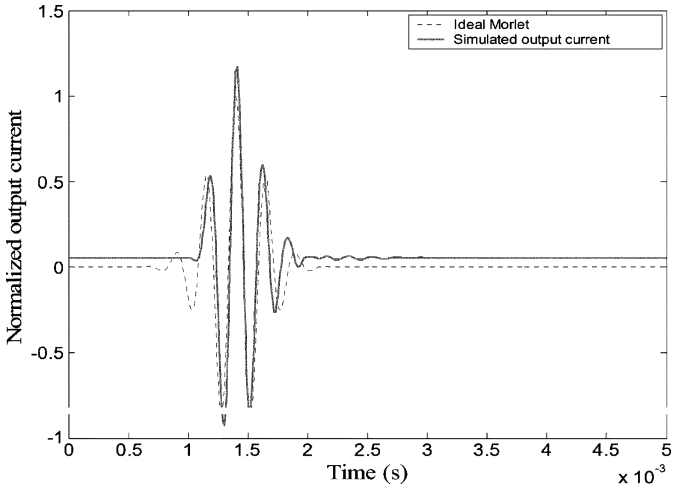

Fig. 9. Simulated impulse response.

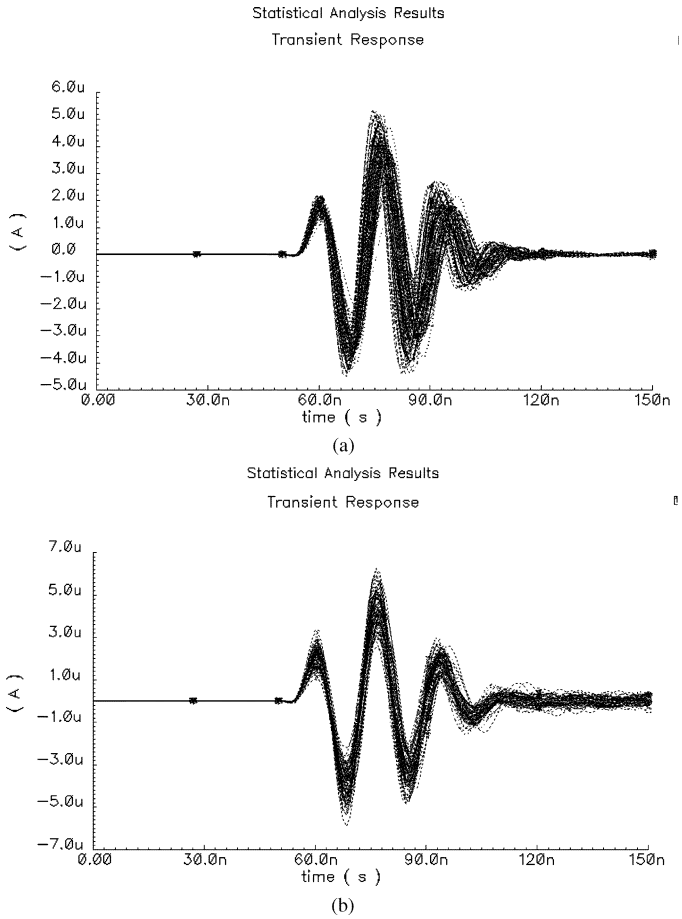

Fig. 10. Monte Carlo analysis. (a) Process variation. (b) Mismatch variation.

the corresponding log-domain integrator with bias current $I_{A_{ij}}$, defined by a current matrix A_I

$$A_I = V_T C_i \cdot A. \tag{17}$$

The input section, as governed by the state-space vector B, can be defined as the input LOG operator and is realized by the first row from the top of Fig. 8. The parameter B is related to the current by

$$B = \frac{I_o}{V_T C_i}. \tag{18}$$

Consequently, the B coefficients are not individually controllable by bias currents, and they have to be set equal to each other (or to zero). Fortunately, this is the case in (15), where only one nonzero parameter of the B vector is present, as then it is not necessary to transpose the state-space system. Finally, in order to restore the overall system linearity one should realize the

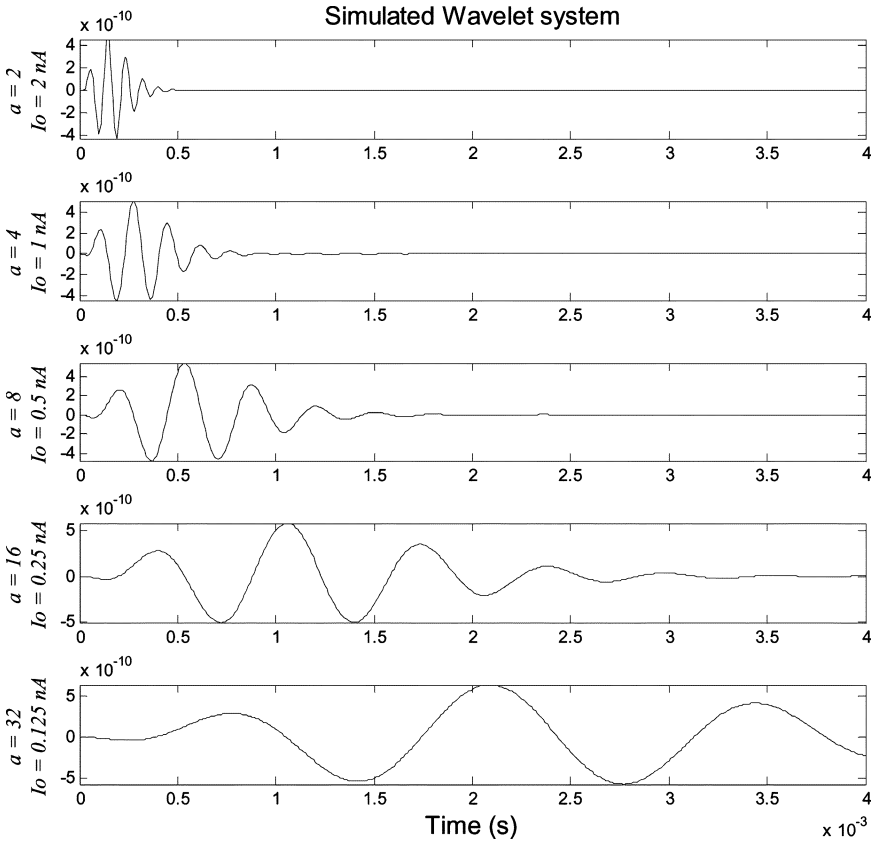

Fig. 11. Simulated impulse responses of a wavelet system with 5 scales. The scales are obtained by varying the current (from 0.125 to 2 nA) or the capacitance (from 100 to 6.25 pF).

weighted summation state with the corresponding EXP operators. Then the bias current vector C_I, which controls the vector C, is defined as

$$C_I = I_o \cdot C. \tag{19}$$

V. Simulation Results

To validate the circuit principle, we have simulated the log-domain state-space filter using models of IBM's 0.18-μm BiCMOS IC technology. The circuit has been designed to operate from a 1.2-V supply. Fig. 9 shows the impulse response of the wavelet filter. The excellent approximation of the Morlet wavelet can be compared with the ideal Morlet function to confirm the performance of the log-domain filter. Fig. 10 shows the Monte Carlo analysis for process and mismatch variation of the technology in use. As evident from the Monte Carlo simulation (i.e., after 100 runs), the system characteristics show insensitivity toward both absolute and relative variations in the process parameters. Even though the impulse response may be slightly affected, the wavelet analysis remains intact.

The total filter's current consumption is 1.5 μA with a 100-pF total capacitance. The output current presents an offset of approximately 46.61 pA. The rms output current noise is 66.97 pA, resulting in a DR at the 1-dB compression point of approximately 30 dB. The power efficiency of any bandpass continuous-time filter is a figure of merit to be able to compare various filter topologies and can be estimated by means of the power dissipation per pole, center frequency (f_c), and quality factor (Q) defined as [18]

$$\text{Power per pole \& bandwidth} = \frac{P_{\text{diss}}}{n \cdot f_c \cdot Q} \tag{20}$$

where P_{diss} is the total power dissipation and n is the order of the filter. The power efficiency of this filter is equal to 11.83 pJ.

In addition, in order to verify the performance of the whole wavelet system, one needs to scale and shift the wavelet base function. By changing the values of the bias currents accordingly, one can obtain a dyadic scale system, as illustrated in Fig. 11. Alternatively, one also may change the capacitance values, C_i. To implement a wavelet system, which usually consists of five dyadic scales, one needs to implement a filter bank (a parallel structure) with a total capacitance of 193.75 pF (capacitance value scaled by a factor of two, i.e., 100 pF for the first scale, 50 pF for the second, 25 pF for the third, 12.5 pF for the fourth, and 6.25 pF for the last scale), preserving the same bias current. This result indicates that the system shown in Fig. 1 is feasible.

Finally, in order to show that the same procedure can be applied for high-frequency applications, we tuned the frequency response of the filter by varying the bias current over about four decades with center frequencies ranging from 5.8 kHz to 58 MHz, while preserving the impulse response waveform. Again, one can obtain the wavelet scales around this frequency (i.e., 58 MHz) by either scaling the current or the capacitance value, accordingly. The performance of the filter is summarized in Table III.

TABLE III
PERFORMANCE PER SCALE FOR TWO DIFFERENT OPERATING FREQUENCIES

Technology	0.18μm BiCMOS	
Bias current	$I_o = 1$nA	$I_o = 10\mu$A
Total capacitance	100pF	100pF
Supply voltage	1.2V	1.8V
Center frequency (f_c)	5.8kHz	58MHz
Power dissipation	1.5 μW	24.3mW
Dynamic Range (1-dB)	30 dB	30 dB
Noise current (rms)	66.97pA	481.3nA
Supply voltage range	1V - 1.6V	1.7V - 2.1V
Power dissipation per pole f_c and Q	11.834pJ	13.96pJ

VI. CONCLUSION

A novel procedure to approximate wavelet bases using analog circuitry was presented. Simulations demonstrated an excellent approximation of the Morlet wavelet base. The filter was optimized with respect to DR. Moreover, sensitivity and sparsity were also taken into account in the design of the filter. Hence, the filter was able to meet the requirements imposed by a low-power environment. The circuit operates from a 1.2-V supply and a bias current of 1.2 μA. From the results obtained, we deduced that this procedure could very well be used to approximate other wavelet bases as well and to implement them on chip in an analog fashion using little power.

ACKNOWLEDGMENT

The authors would like to thank R. Westra, R. Peeters, and J. Karel from the University of Maastricht for the useful discussions; and D. Harame and IBM Microelectronics for fabrication access.

REFERENCES

[1] I. Daubechies, *Ten Lectures on Wavelets*. Philadelphia, PA: SIAM, 1992.
[2] S. Mallat, *A Wavelet Tour of Signal Processing*. New York: Academic, 2001.
[3] O. Rioul and M. Vetterli, "Wavelets and signal processing," *IEEE Signal Process. Mag.*, vol. 8, no. 4, pp. 14–38, Oct. 1991.
[4] S. A. P. Haddad, R. Houben, and W. A. Serdijn, "Analog wavelet transform employing dynamic translinear circuits for cardiac signal characterization," in *Proc. IEEE Int. Symp. Circuits and Systems*, vol. 1, May 2003, pp. 121–124.
[5] J. S. Sahambi, S. N. Tandon, and R. K. P. Bhatt, "Using wavelet transform for ecg characterization," *IEEE Eng. Med. Biol.*, pp. 77–83, Feb. 1997.
[6] M. Unser and A. Aldroubi, "A review of wavelets in biomedical applications," *Proc. IEEE*, vol. 84, no. 4, pp. 626–638, Apr. 1996.
[7] S. A. P. Haddad and W. A. Serdijn, "Mapping the wavelet transform onto silicon: the dynamic translinear approach," in *Proc. IEEE Int. Symp. Circuits and Systems*, vol. 5, May 2002, pp. 621–624.
[8] D. Zwillinger, *Standard Mathematical Tables and Formulae*, 30th ed. Boca Raton: CRC, 1996.
[9] K. L. Su, *Time Domain Synthesis of Linear Networks*. Englewood Cliffs, NJ: Prentice-Hall, 1971.
[10] G. A. Baker Jr., *Essentials of Pade Approximants*. New York: Academic, 1975.
[11] L. Thiele, "On the sensitivity of linear state-space systems," *IEEE Trans. Circuits Syst.*, vol. CAS-33, no. 5, pp. 502–510, May 1986.
[12] W. M. Snelgrove and A. S. Sedra, "Synthesis and analysis of state-space active filters using intermediate transfer function," *IEEE Trans. Circuits Syst.*, vol. CAS-33, no. 3, pp. 287–301, Mar. 1986.
[13] D. P. W. M. Rocha, "Optimal design of analogue low-power systems, a strongly directional hearing-aid adapter," Ph.D. thesis, Delft University of Technology, Delft, The Netherlands, Apr. 2003.
[14] D. A. Johns, W. M. Snelgrove, and A. S. Sedra, "Orthonormal ladder filters," *IEEE Trans. Circuits Syst.*, vol. 36, no. 3, pp. 337–343, Mar. 1989.
[15] G. Groenewold, "Optimal dynamic range integrators," *IEEE Trans. Circuits Syst. I, Fundam. Theory Appl.*, vol. 39, no. 8, pp. 614–627, Aug. 1992.
[16] M. N. El-Gamal and G. W. Roberts, "A 1.2 v npn-only integrator for log-domain filtering," *IEEE Trans. Circuits Syst. II, Anal. Digit. Signal Process.*, vol. 49, no. 4, pp. 257–265, Apr. 2002.
[17] G. W. Roberts and V. W. Leung, *Design and Analysis of Integrator-Based Log-Domain Filter Circuits*. Dordrecht, The Netherlands: Kluwer, 2000.
[18] C. Toumazou, G. Moschytz, and B. Gilbert, *Trade-Offs in Analog Circuit Design*. Dordrecht, The Netherlands: Kluwer, 2002.

Sandro A. P. Haddad (S'99) was born in Anápolis, Brazil, in 1977. He received the B.Eng. degree from the University of Brasília (UnB), Brasília, Brazil, in 2000, with honors. He is working toward the Ph.D. degree at the Electronics Research Laboratory, Delft University of Technology, Delft, The Netherlands, since 2001

His research is a part of the Biomedical Signal Processing Platform for Low-Power Real-Time Sensing of Cardiac Signals (BioSens). His research interests include low-voltage, ultra low-power analog electronics and biomedical systems, and high-frequency analog integrated circuits for ultra-wide band communications.

Sumit Bagga (S'03) was born in New Delhi, India, in 1977. He received the B.S. and M.E. degrees in electrical engineering from Shivaji University, Kolhapur, India, and University of Brasília, Brasília, Brazil in 1999 and 2002, respectively.

In November 2002, he joined the Electronics Research Laboratory (EEMCS), Delft University of Technology, Delft, The Netherlands, where he is involved with designing transceiver architectures and circuits for ultra-wide band communications in the AIRLINK project under the FREEBAND initiative. His research interests include high-speed, low-power analog circuit design.

Mr. Bagga received the Best Paper Award from UWBST and IWUWBS 2004.

Wouter A. Serdijn (M'98) was born in Zoetermeer The Netherlands, in 1966. He received the "ingenieurs" (M.Sc.) degree in electrical engineering and the Ph.D. degree in elctronics from the Delft University of Technology, Delft, The Netherlands, in 1989 and 1994, respectively.

Since 1997, he is a Project Leader in the multi-disciplinary Ubiquitous Communications (UbiCom) research program of the Delft University of Technology. In 2002, he became a workpackage leader in the Freeband Impulse project AIR-LINK, aiming at high-quality, wireless short-distance communication, employing ultra-wide band (UWB) radio. His research interests include low-voltage, ultra-low-power, high-frequency and dynamic-translinear analog integrated circuits along with circuits for RF and UWB wireless communications, hearing instruments and pacemakers. He is co-editor and coauthor of the books *Research Perspectives on Dynamic Translinear and Log-Domain Circuits* (Norwell, MA: Kluwer, 2000), *Low-Voltage Low-Power Analog Integrated Circuits* (Norwell, MA: Kluwer, 1995) and *Dynamic Translinear and Log-Domain Circuits* (Norwell, MA: Kluwer, 1998). He authored and coauthored more than 150 publications and presentations. He teaches analog electronics for electrical engineers, micropower analog ic design and electronic design techniques.

Dr. Serdijn received the EE Best Teacher Award in 2001 and 2004. He has served as an Associate Editor of the IEEE TRANSACTIONS ON CIRCUITS AND SYSTEMS—II: ANALOG DIGITAL SIGNAL PROCESSING, and currently serves as an Associate Editor of the IEEE TRANSACTIONS ON CIRCUITS AND SYSTEMS—I: FUNDAMENTAL THEORY AND APPLICATIONS. He served as Tutorial Session Co-chair (with A. Andreou) for the International Symposium on Circuits and Systems (ISCAS) 2003, as Analog Signal Processing Track Co-Chair (with T. Tarim and I. Filanovsky) for ISCAS 2004, as Chair of the Analog Signal Processing Technical Chapter of the IEEE CAS society, as Analog Signal Processing Track Co-Chair for the International Conference Electronics Circuits and Systems (ICECS) 2004, as Technical Program Committee member for the 2004 International Workshop on Biomedical Circuits and Systems, and is currently serving as Analog Signal Processing Track Co-Chair (with U. K. Moon and I. Filanovsky) for ISCAS 2005.